

A Spectroscopic Study on the Nitrogen Electrochemical Reduction Reaction on Gold and Platinum Surfaces

Yao Yao,^{†,§} Shangqian Zhu,[†] Haijiang Wang,^{||} Hui Li,[§] and Minhua Shao^{*,†,‡,||}

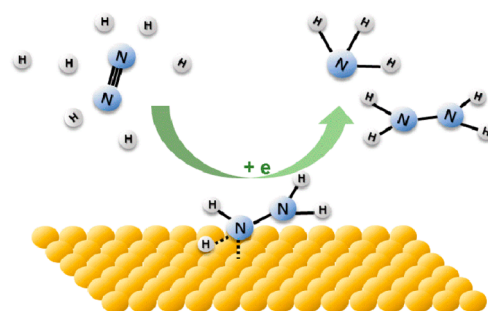
[†]Department of Chemical and Biological Engineering, and [‡]Energy Institute, The Hong Kong University of Science and Technology, Clear Water Bay, Kowloon, Hong Kong

[§]Department of Materials Science and Engineering, and ^{||}Department of Mechanical and Energy Engineering, South University of Science and Technology of China, 1088 Xueyuan Boulevard, Nanshan District, Shenzhen, Guangdong 518055, China

Supporting Information

ABSTRACT: The electrochemical reduction of nitrogen to ammonia on Au-based catalysts showed a reasonably high Coulombic efficiency. The pathway of this promising reaction, however, is not clear partially due to the lack of information on reaction intermediates. Herein, surface-enhanced infrared absorption spectroscopy (SEIRAS) was employed to study the reaction mechanisms of nitrogen reduction on an Au thin film for the first time. During the nitrogen reduction, the N_2H_x species was detected with bands at 1453 (H–N–H bending), 1298 (–NH₂ wagging), and 1109 cm⁻¹ (N–N stretching) at potentials below 0 V against reversible hydrogen electrode. This result indicates that the nitrogen reduction reaction on Au surfaces follows an associative mechanism, and the N≡N bond in N₂ tends to break simultaneously with the hydrogen addition. By comparison, no absorption band associated with N was observed on Pt surfaces under the same reaction condition. This result is consistent with the low efficiency of nitrogen reduction on Pt due to the much faster kinetics of hydrogen evolution reaction.

Nitrogen Electrochemical Reduction on Au



INTRODUCTION

Ammonia has received much attention as a potential energy storage medium and an alternative fuel for vehicles, in addition to its use as a kind of nitrogen fertilizers in the anhydrous, solution, or salt form.^{1,2} In 2015, the production of ammonia consumed 2% of the global annual energy and was responsible for 0.5% of the CO₂ emission.^{3,4} Recent studies showed that ammonia could be produced by N₂ and H₂O through an electrochemical method, with the advantages of zero CO₂ emission and energy saving as compared to the Haber–Bosch process.^{5–9} However, as the theoretical potentials of hydrogen evolution reaction (HER) and nitrogen reduction reaction (NRR) are very close, H₂ is the dominant product due to the much faster reaction kinetics of the former. Theoretical computation results demonstrated that the adsorption of reactants and proton/electron transfer were not favorable on most catalyst surfaces during NRR.^{10,11} Up to now, the highest Coulombic efficiency in the ammonia electrochemical synthesis systems is about 35%, realized at ~200 °C by using molten hydroxide as the electrolyte and Fe₂O₃ nanoparticles as the electrocatalyst.¹² In addition to the low Coulombic efficiency, the extremely slow formation rate of ammonia is another big issue. The highest reaction rate for ammonia electrochemical synthesis is ~1 × 10⁻⁸ mol_{NH₃} s⁻¹ cm⁻²,^{7,12,13} which is much lower than the common ammonia production rate of commercial systems.¹⁴ Under the ambient condition, the situation is even worse with the highest ammonia formation

rate of ~1.14 × 10⁻⁹ mol_{NH₃} s⁻¹ cm⁻²,¹⁵ achieved in a proton exchange membrane-based system by using Pt/C as the catalyst. The highest Coulombic efficiency of 8.11% was obtained in an alkaline system with TiO₂–Au as the catalyst.⁶ Although Au itself is not a good NRR catalyst as predicted by theoretical calculations,^{10,16} the synergetic effect from the TiO₂ substrate may boost the NRR activity.

There are two main reaction pathways, dissociative and associative mechanisms, during ammonia synthesis. In the former, the N≡N bond is broken into nitrogen atoms on catalyst surfaces before the addition of hydrogen. In the latter, the N≡N bond of the nitrogen molecule is broken simultaneously with the addition of hydrogen. It is generally believed that the dissociative mechanism is dominant in the Haber–Bosch process.¹⁰ Despite that understanding the NRR mechanism is vital for the rational design of more advanced electrocatalysts, the experimental studies in this area are rather rare due to the significant influence of HER. The aim of this study is to understand the NRR mechanism on an Au electrode by detecting reaction intermediates with the powerful surface-enhanced infrared absorption spectroscopy (SEIRAS) technique.^{17–23} Au was selected because of its low HER activity.^{6,24} Therefore, the influence of HER on the measurements was minimized.

Received: November 15, 2017

Published: January 10, 2018

RESULTS AND DISCUSSION

The cyclic voltammogram (CV) of an Au thin film in a N_2 -saturated KOH solution is shown in Figure 1. In the first

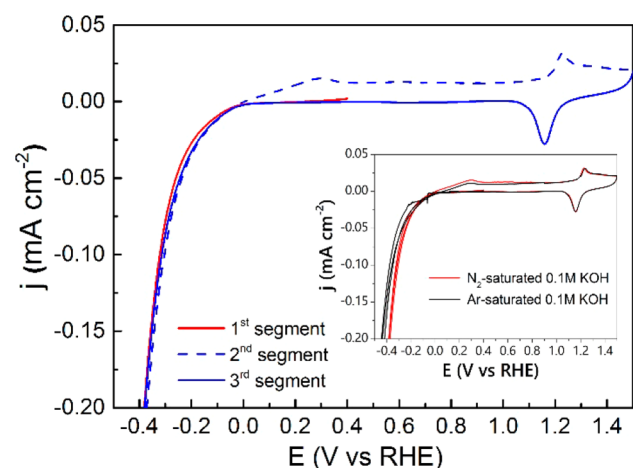


Figure 1. Cyclic voltammograms of an Au film electrode deposited on the Si prism in a N_2 -saturated 0.1 M KOH aqueous solution. First segment, cathodic scan from 0.4 to -0.5 V; second segment, anodic scan from -0.5 to 1.5 V; third segment, cathodic scan from 1.5 to -0.5 V. Inset: Comparisons of CVs of the Au film in N_2 - (red lines) and Ar-saturated (black lines) 0.1 M KOH solutions. An Hg/HgO electrode was used as the reference. Potential scan rate: 2.5 mV s^{-1} .

segment (cathodic scan, solid red line), the reduction current resulting from the HER and NRR appeared at 0 V and rose sharply starting at -0.1 V. In the following backward scan (dashed blue line), a weak oxidation current peak was observed at 0.28 V, which may mainly result from the oxidation of hydrogen. With the potential increased to 1.1 V, an obvious oxidation current appeared associated with Au surfaces' oxidation. In the third segment (solid blue line), the reduction of Au oxides resulted in a current peak at 1.1 V, which is consistent with the literature.²⁵ When the potential decreased to -0.1 V, a reduction current similar to that in the first segment appeared. The CV of the same Au electrode in an Ar-saturated KOH solution is shown in Figure S1 for comparison. A similar oxidation current peak was also observed at 0.28 V in the second segment, confirming that it was mainly associated with hydrogen oxidation rather than oxidation of N-containing species generated at low potentials. This result is also consistent with the fact that the amount of ammonia produced in the cathodic scan was very small. The inset of Figure 1 compares CVs of the Au film in N_2 - (red lines) and Ar-saturated (black lines) 0.1 M KOH solutions. The reduction current density below -0.1 V in the former is slightly larger than that in the latter, implying that the Au thin film may catalyze the NRR. To confirm the formation of ammonia at negative potentials, we employed an indophenol method using an ammonia meter (Palintest PTH 042) to measure the amount of ammonia produced at negative potentials. As the Au thin film deposited on the Si prism can be easily peeled off in a long-term testing in the alkaline electrolyte, an Au foil with a geometric area of 5 cm^2 sputtered with a 50 nm-thick Au film was used as the working electrode instead. After keeping the potential at -0.5 V for 10 h, the concentration of ammonia in the electrolyte was determined to be 0.14 ppm, corresponding to an ammonia

formation rate of $\sim 3.84 \times 10^{-12} \text{ mol cm}^{-2} \text{ s}^{-1}$ and a Faradaic efficiency of 0.12%.

To identify possible reaction intermediates during the potential cycling in Figure 1, SEIRAS measurements were conducted. Figure 2a shows the IR spectra collected in the first

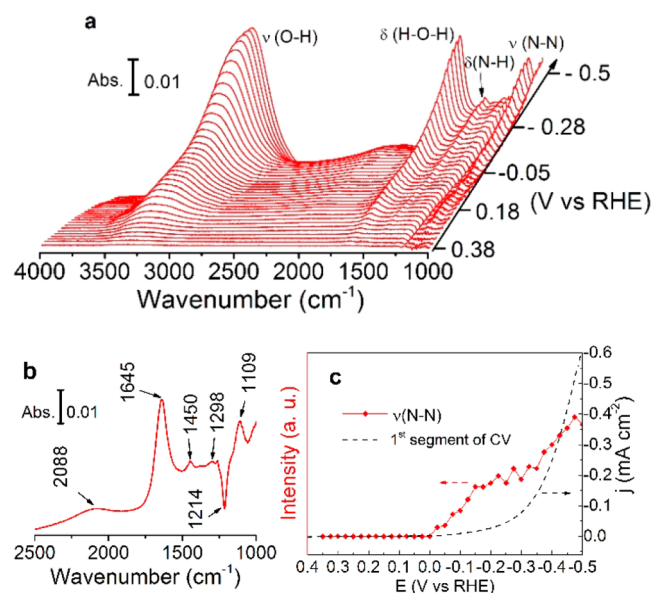


Figure 2. (a) FTIR spectra during the first segment from 0.4 to -0.5 V on the Au film electrode in a N_2 -saturated 0.1 M KOH solution. The reference spectrum was taken at 0.4 V. (b) The single spectrum at -0.5 V in the range of $1000\text{--}2500 \text{ cm}^{-1}$. (c) The potential dependence of the IR absorption band of N–N stretching derived from (a). The corresponding first segment of the CV (black dashed line) in N_2 -saturated 0.1 M KOH is also shown.

CV segment with the spectrum at 0.4 V as the reference. The IR bands at 3300 and 1645 cm^{-1} are attributed to the O–H stretching and H–O–H bending of water molecules, respectively.^{17,26} The intensity of those two bands increased as the potential became more negative. It is well-known that water molecules are adsorbed on the electrode surface with an ice-like structure paralleling with the surface at potential of zero charge (PZC).¹⁷ Therefore, the intensities of IR bands of adsorbed water are the weakest at PZC. Shifting the potential in the negative or positive direction would change the orientation of water molecules on the electrode, resulting in an increase of the intensities of IR bands.¹⁷ A broad positive band at $\sim 2088 \text{ cm}^{-1}$ that appeared with the reduction current in Figure 1 is attributed to the adsorbed H atoms.^{27,28} The negative-going band at $\sim 1214 \text{ cm}^{-1}$ is associated with Si–O from the Si prism.²⁹ Three weak bands at 1450, 1298, and 1109 cm^{-1} are attributed to the H–N–H bending,^{30–32} $-\text{NH}_2$ wagging,^{32,33} and N–N stretching^{32,34} of adsorbed N_2H_y species, respectively. The stark effect of these bands is not significant as in previous studies on other adsorbates.^{35–37} These bands can be clearly revealed in a single spectrum at -0.5 V shown in Figure 2b. The bands at 1450 and 1289 cm^{-1} were also reported on N_2H_4 on a Pt surface in KOH solution.³⁸ Figure 2c shows the potential dependence of the strongest band among the three (N–N stretching at 1109 cm^{-1}) and the corresponding first segment of the CV (black dashed line). The band started to appear at potentials below 0 V and increased with potential decreasing, accompanied by the increase of the reduction current in the first segment of the CV.

To further confirm the band assignments, the IR spectrum of 0.7 M $\text{NH}_3 \cdot \text{H}_2\text{O}$ in a KOH solution was collected after subtracting the background spectrum of 0.1 M KOH using a ZnSe prism. As shown in Figure S2a (black line), the positive bands at ~ 3397 and ~ 2972 cm^{-1} were attributed to the N–H stretching of ammonia in the solution.³⁹ The strong negative-going bands at ~ 3300 and ~ 1635 cm^{-1} were attributed to overlapping of N–H/O–H stretching and bending of H–N–H/H–O–H. The negative-going bands were caused by the less absorptivity of the N–H bond than that of the O–H bond.³⁹ N–H bonds are less polar and form weaker hydrogen bonds than O–H, resulting in a weaker infrared absorption.⁴⁰ For the same reason, these two bands became more negative when the concentration of ammonia increased from 0.7 to 1.0 M (red line). The positive-going band at ~ 1110 cm^{-1} was assigned to the NH_3 symmetric deformation and increased with the ammonia concentration.³⁹ The difference between 0.7 and 1.0 M $\text{NH}_3 \cdot \text{H}_2\text{O}$ in IR absorption can be clearly observed in the subtractive spectrum (the difference between the spectra at 1.0 and 0.7 M) shown in Figure S2b. As the ammonia formation rate on Au surface under the ambient condition is extremely low, we do not expect a significant amount of ammonia in the solution during the potential scan. As a result, the band at ~ 1109 cm^{-1} in Figure 2 should be attributed to the adsorbent (N_2H_y) on the Au surface rather than ammonia in the bulk solution.

When the same spectra were collected using the Au-coated Si as the prism, an additional positive band at ~ 1444 cm^{-1} was observed in the subtractive spectrum (Figure S3). This band should be related to the H–N–H bending of adsorbed NH_x species on the Au surface. The appearance of the H–N–H bending and N–N stretching bands indicates that the N_2H_y ($2 \leq y \leq 4$) species were formed on the Au surface at potentials below 0 V. Our results imply that the electrochemical NRR on an Au surface follows an associative mechanism under the current reaction condition. This conclusion is very reasonable as it is difficult to break the $\text{N}\equiv\text{N}$ triple bond without adding hydrogen atoms at room temperature. A recent study also demonstrated that N_2H_4 is one of the products for nitrogen electrochemical reduction on Au NPs in alkaline solution.²⁴ To further confirm that the IR bands at 1450, 1298, and 1109 cm^{-1} belong to the vibration of N_2H_y -related bonds rather than contaminants, IR spectra in the Ar-saturated electrolyte in the first segment were also collected under the same conditions. As shown in Figure 3a and b, only the water-related bands and the Au–H stretching at ~ 2090 cm^{-1} ^{127,28} were observed. SEIRAS measurements in both N_2 - and Ar-saturated 0.1 M KOH solutions were repeated for more than 10 times, and similar results were observed as in Figures 2 and 3. Two of the repeats are shown in Figure S4 (in N_2 -saturated solution) and Figure S5 (in Ar-saturated solution).

Next, we monitored the evolution of reaction intermediates during the positive-going scan (the second segment in Figure 1). Figure 4 shows selected spectra at -0.45 , 0.0, 0.5, and 1.0 V with the spectrum at -0.5 V as the reference. Again, the negative-going bands associated with the H–O–H bending (~ 1635 cm^{-1}) and O–H stretching (~ 3240 cm^{-1}) appeared as a result of the change in the adsorption configuration of water molecules upon increasing the potential.¹⁷ The broad band at ~ 2088 cm^{-1} attributed to adsorbed H atoms also became negative at 0.5 V due to hydrogen oxidation. The same phenomenon was also detected in the second segment from -0.5 to 1.0 V in an Ar-saturated 0.1 M KOH solution, shown in

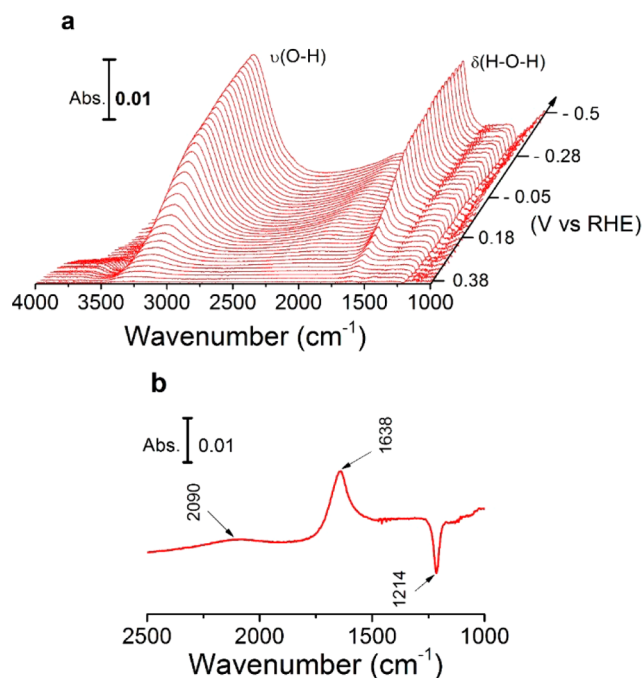


Figure 3. (a) FTIR spectra collected in the first scan from 0.4 to -0.5 V on the Au film electrode in an Ar-saturated 0.1 M KOH aqueous solution. The background spectrum was taken at 0.4 V. (b) The single spectrum at -0.5 V in the range of 1000 – 2500 cm^{-1} .

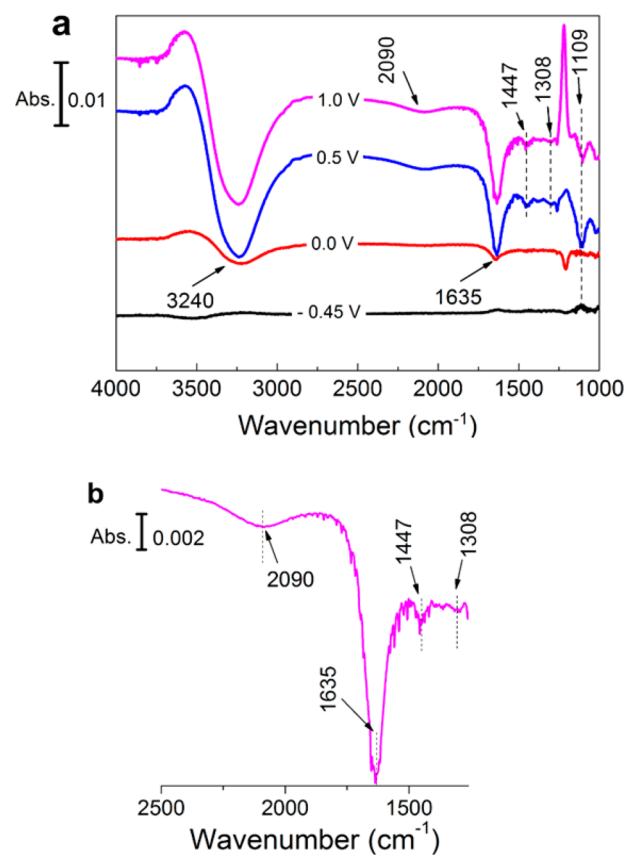


Figure 4. (a) FTIR spectra recorded in the second segment of the CV in Figure 1 from -0.5 to 1.0 V; the reference spectrum was taken at -0.5 V. (b) The enlarged spectrum at 1.0 V in the range of 1260 – 2500 cm^{-1} .

Figure S6. Negative-going bands related to N_2H_y species including the H–N–H bending at $\sim 1447\text{ cm}^{-1}$, $-NH_2$ wagging at $\sim 1308\text{ cm}^{-1}$, and N–N stretching at $\sim 1109\text{ cm}^{-1}$ started to appear at 0.5 V (the blue line). These weak peaks could be seen more clearly in the enlarged spectrum at 1.0 V in **Figure 4b**. The IR result suggests that the N_2H_y species could be removed by oxidization at potentials around this potential. This result is consistent with the previous study showing that hydrazine could be oxidized on Au surfaces at $\sim 0.5\text{ V}$ in alkaline solutions.⁴¹ Because of the very limited amount of adsorbed N_2H_y species on Au surfaces and interference from hydrogen oxidation, the removal of these species did not result in a visible current peak. With the potential increased to 1 V, the negative band at $\sim 1109\text{ cm}^{-1}$ became weaker. It is caused by the OH adsorption on the Au surfaces at high potentials that gives a positive band at $\sim 1130\text{ cm}^{-1}$ due to the librational mode of OH_{ad} .⁴² The overlapping of this band with the N–N stretching at 1109 cm^{-1} resulted in a weaker band than that at 0.5 V. The bands at ~ 1057 and 1210 cm^{-1} observed at 0.5 and 1.0 V are associated with Si–O from the Si prism.^{29,43}

It will be of interest to compare the NRR reaction mechanisms on Pt and Au as the former is an excellent catalyst toward HER. The selected FTIR spectra of Pt thin film during the negative-going scan from 0.4 to -0.1 V in N_2 -saturated 1.0 M KOH, with the spectrum at 0.4 V as the reference, are shown in **Figure 5**. The corresponding CV of Pt is shown in **Figure S7**.

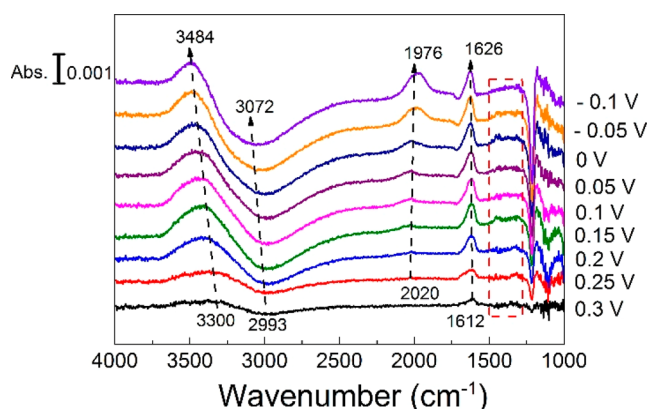


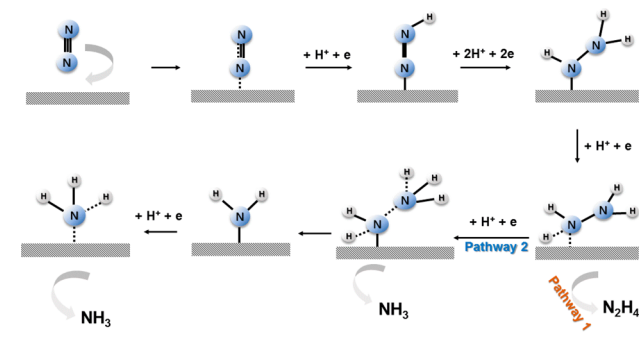
Figure 5. FTIR spectra during the negative scan from 0.4 to -0.1 V on a Pt film electrode in a N_2 -saturated 0.1 M KOH solution. The reference spectrum was taken at 0.4 V; potential scan rate: 2.5 mV s^{-1} .

With the potential decreasing, the band intensities of H–O–H bending at $1612\text{--}1626\text{ cm}^{-1}$ and O–H stretching at $3300\text{--}3484\text{ cm}^{-1}$ increase due to the change of the adsorption configuration of water on Pt surfaces,¹⁷ which is similar to the observation on Au surfaces in **Figure 2a**. The band at $2993\text{--}3072\text{ cm}^{-1}$ is attributed to the O–H stretching of the second water layer in ice-like structure on Pt surface.⁴⁴ While decreasing the potential from 0.4 to -0.1 V , the intensity of the O–H stretching of the second water layer decreased with the breakdown of the ice-like structure of the water. The band at $2020\text{--}1976\text{ cm}^{-1}$ is attributed to the H atom adsorbed on Pt.^{45,46} Its intensity increased and shifted to a lower wavenumber with the decrease of potential, which is in accordance with previous studies.⁴⁶ Again, the negative-going band at $\sim 1214\text{ cm}^{-1}$ is associated with Si–O from the Si prism.²⁹ Interestingly, the range between ~ 1300 and 1500 cm^{-1} is featureless in **Figure 5**. This observation can be due to the

low Faradaic efficiency of NRR on Pt surfaces as compared to HER resulting in a much lower signal from N_2H_y if there is any.

On the basis of the in situ SEIRAS data, we may deduce the possible NRR pathway on Au surfaces, as shown in **Scheme 1**.

Scheme 1. Nitrogen Electrochemical Reduction Reaction Pathway on Au Surface



At potentials around -0.1 V or lower, the N_2 molecule is adsorbed on Au surfaces followed by proton and electron transfer forming $*N_2H_y$ ($1 < y < 4$) species (* represents adsorbed species). In **Figure 2**, the appearance of IR absorption bands at 1453 cm^{-1} (H–N–H bending), 1298 cm^{-1} ($-NH_2$ wagging), and 1109 cm^{-1} (N–N stretching) at potentials below 0 V (RHE) suggests the formation of $*N_2H_y$ ($1 < y < 4$) on the Au surface at these potentials. When $*N_2H_4$ is formed, there are two possible consequent pathways. In pathway 1 involving four-electron transfer, the $*N_2H_4$ is desorbed from the Au surface entering into the solution. A recent study illustrates that hydrazine is a kind of byproduct of NRR on Au surface in a KOH solution.²⁴ In pathway 2 involving six-electron transfer, further reduction occurs with NH_3 being the final product. With one proton and electron transferred to $*N_2H_4$, a free NH_3 molecule is formed together with $*NH_2$. By adding another proton and electron on $*NH_2$, the second NH_3 molecule can be produced. The formation of NH_3 was also supported in our electrolysis experiment at -0.5 V .

CONCLUSION

In summary, the NRR on an Au thin film was studied by the powerful surface-sensitive SEIRAS technique for the first time. During the nitrogen reduction, the adsorbed N_2H_y was detected with bands of the H–N–H bending at 1453 cm^{-1} , the $-NH_2$ wagging at 1298 cm^{-1} , and the N–N stretching at 1109 cm^{-1} at potential below 0 V (RHE). On the basis of this result, an associative reaction mechanism on Au surfaces was proposed. The $N\equiv N$ bond tends to break simultaneously with the hydrogen and electron addition by forming N_2H_y . During the anodic scan, the adsorbed N_2H_y could be oxidized at potential around 0.5 V. By comparison, those bands were not observed on Pt surfaces under the same conditions, consistent with the low efficiency of NRR due to the much faster kinetics of HER on Pt. Our results add significant new insights into the reaction mechanisms of NRR on metal surfaces and may guide rational design of more advanced electrocatalysts.

EXPERIMENTAL SECTION

Synthesis of the Thin-Film Gold Electrode. The Au film was deposited by a chemical process, which was described specifically in previous literature.⁴⁷ The Si prism (20 mm in diameter, MTI Corp.) surface was polished with Al_2O_3 powder and cleaned in water with

sonication. The prism then was soaked in a piranha solution (3:1 volumetric ratio of 98% H₂SO₄ (Aldrich) and 30% H₂O₂ (Aldrich)) for 2 h. The reflection plane was then treated by 40% NH₄F (Aldrich) for 90 s, and immersed in a mixture of 4 mL of Au plating solution⁴⁸ and 50 μL of 50% HF solution (Aldrich) at 55 °C for 5 min.

Synthesis of the Thin-Film Platinum Electrode. Pt thin film was electrodeposited on the synthesized Au film by employing galvanostatic mode at room temperature. The plating solution consisted of 4 mM H₂PtCl₆ (Aldrich) and 0.7 M Na₂HPO₄ (VWR Chemicals), and the depositing current and duration were 1.5 mA and 450 s, respectively.

The Au or Pt thin film that was supported on the Si prism was used as the working electrode (WE), with a geometrical surface area of 1.76 cm². A Pt foil and a Hg/HgO electrode were used as counter and reference electrodes, respectively. The supporting electrolyte used in all measurements was 0.1 M KOH (99.99%, Aladdin) or 1 M KOH, which was constantly purged with N₂ or Ar (5N, Air Products and Chemicals (Shenzhen), Inc.) during the experiment. All potentials in this study were referred to the reversible hydrogen electrode (RHE) scale.

Electrochemical ATR-FTIR Measurements. The cell used for ATR-FTIR measurements in this study is the same as what has been reported earlier.⁴⁹ Before the experiment, the WE was cleaned by electrochemical method. When using Au film as the WE, the Au thin film was cleaned by continuously scanning the potential from 0.2 to 1.5 V for ca. 8 min in 0.1 M KOH. The electrode potential then was scanned between -0.5 and 1.5 V at a scan rate of 2.5 mV s⁻¹. Meanwhile, IR spectra were recorded with a time resolution of 10 s per spectrum at a spectral resolution of 4 cm⁻¹. All spectra were presented in absorbance, $A = -\log(R/R_0)$, where R is the reflectance of the sample spectrum and R_0 is the background spectrum. When using the Pt film as WE, it was cleaned by continuously scanning the potential from 0.05 to 1 V for ca. 8 min in 1 M KOH. The electrode potential then was scanned between 0.4 and -0.1 V at a scan rate of 2.5 mV s⁻¹. Other conditions are the same as those of the Au film. A Nicolet iS50 FT-IR spectrometer was used. The electrochemical characterization was performed with a CHI 760E electrochemical workstation.

Measurement of NRR Faradaic Efficiency of Au Film. The ammonia produced on Au surfaces during NRR was detected by the indophenol method with an ammonia meter (Palintest PTH 042). The calibration curve for the ammonia meter is shown in Figure S8. As the Au thin film deposited on the Si prism can be easily peeled off in a long-term testing in the alkaline electrolyte, an Au foil with a geometric area of 5 cm² sputtered with a 50 nm-thick Au film was used as the working electrode instead. A carbon rod and a Hg/HgO were used as the counter and reference electrodes, respectively. The electrolyte was a N₂-saturated 0.1 M KOH solution with a volume of 83 mL. Figure S9 is the current–time response at -0.5 V for 10 h. After the electrolysis, the ammonia in the electrolyte was measured by the ammonia meter. The ammonia formation rate (r) and Faradaic efficiency (FE) could be calculated by the following equations:

$$r(\text{NH}_3) = \frac{[\text{NH}_3] \times V}{t \times A}$$

$$\text{FE}(\text{NH}_3) = \frac{Q_{\text{NH}_3}}{Q_{\text{total}}} = \frac{3 \times 96500 \times [\text{NH}_3] \times V}{\int i \, dt}$$

■ ASSOCIATED CONTENT

● Supporting Information

The Supporting Information is available free of charge on the ACS Publications website at DOI: 10.1021/jacs.7b12101.

Detailed information on the CV and FTIR spectra of Au film in an Ar-saturated KOH electrolyte, infrared spectroscopy of ammonia–water, the CV of Pt film in a N₂-saturated KOH electrolyte, the calibration curve of

the ammonia meter, the current–time plot of the Au foil, and the repeated FTIR experiment on NRR (PDF)

■ AUTHOR INFORMATION

Corresponding Author

*kemshao@ust.hk

ORCID

Shangqian Zhu: 0000-0002-5813-9588

Minhua Shao: 0000-0003-4496-0057

Notes

The authors declare no competing financial interest.

■ ACKNOWLEDGMENTS

We acknowledge support from the Research Grant Council (26206115), the Guangdong Special Fund for Science and Technology Development - Hong Kong Technology Cooperation Funding Scheme (201604030012, 201704030065), a startup fund from the Hong Kong University of Science and Technology, and the Shenzhen Key Laboratory project (ZDSYS201603311013489).

■ REFERENCES

- (1) Lan, R.; Irvine, J. T. S.; Tao, S. W. *Int. J. Hydrogen Energy* **2012**, *37*, 1482–1494.
- (2) Rees, N. V.; Compton, R. G. *Energy Environ. Sci.* **2011**, *4*, 1255–1260.
- (3) Varotto, A. Raising the standrads: Enhanced catalytic performance for global ammonia production, 2015.
- (4) European Commission. Large Volume Inorganic Chemicals - Ammonia, Acids and Fertilisers, 2007.
- (5) Kim, K.; Yoo, C. Y.; Kim, J. N.; Yoon, H. C.; Han, J. I. *Korean J. Chem. Eng.* **2016**, *33*, 1777–1780.
- (6) Shi, M. M.; Bao, D.; Wulan, B. R.; Li, Y. H.; Zhang, Y. F.; Yan, J. M.; Jiang, Q. *Adv. Mater.* **2017**, *29*, 1606550.
- (7) Murakami, T.; Nohira, T.; Goto, T.; Ogata, Y. H.; Ito, Y. *Electrochim. Acta* **2005**, *50*, 5423–5426.
- (8) McEnaney, J. M.; Singh, A. R.; Schwab, J. A.; Kibsgaard, J.; Lin, J. C.; Cargnello, M.; Jaramillo, T. F.; Nørskov, J. K. *Energy Environ. Sci.* **2017**, *10*, 1621–1630.
- (9) Chen, G. F.; Cao, X. R.; Wu, S. Q.; Zeng, X. Y.; Ding, L. X.; Zhu, M.; Wang, H. H. *J. Am. Chem. Soc.* **2017**, *139*, 9771–9774.
- (10) Montoya, J. H.; Tsai, C.; Vojvodica, A.; Nørskov, J. K. *ChemSusChem* **2015**, *8*, 2180–2186.
- (11) Skúlason, E.; Bligaard, T.; Gudmundsdóttir, S.; Studt, F.; Rossmeisl, J.; Abild-Pedersen, F.; Vegge, T.; Jonsson, H.; Nørskov, J. K. *Phys. Chem. Chem. Phys.* **2012**, *14*, 1235–1245.
- (12) Licht, S.; Cui, B. C.; Wang, B. H.; Li, F. F.; Lau, J.; Liu, S. Z. *Science* **2014**, *345*, 637–640.
- (13) Li, F. F.; Licht, S. *Inorg. Chem.* **2014**, *53*, 10042–10044.
- (14) Giddey, S.; Badwal, S. P. S.; Kulkarni, A. *Int. J. Hydrogen Energy* **2013**, *38*, 14576–14594.
- (15) Lan, R.; Irvine, J. T. S.; Tao, S. W. *Sci. Rep.* **2013**, *3*, 1145.
- (16) Höskuldsson, A. r. B.; Abghoui, Y.; Gunnarsdóttir, A. B.; Skúlason, E. *ACS Sustainable Chem. Eng.* **2017**, *5*, 10327–10333.
- (17) Ataka, K.; Yotsuyanagi, T.; Osawa, M. *J. Phys. Chem.* **1996**, *100*, 10664–10672.
- (18) Chen, Y. X.; Miki, A.; Ye, S.; Sakai, H.; Osawa, M. *J. Am. Chem. Soc.* **2003**, *125*, 3680–3681.
- (19) Yao, Y.; Chen, W.; Du, Y. X.; Tao, Z. C.; Zhu, Y. W.; Chen, Y. X. *J. Phys. Chem. C* **2015**, *119*, 22452–22459.
- (20) Osawa, M.; Ataka, K.; Yoshii, K.; Nishikawa, Y. *Appl. Spectrosc.* **1993**, *47*, 1497–1502.
- (21) Osawa, M. Surface-Enhanced Infrared Absorption. In *Near-Field Optics and Surface Plasmon Polaritons*; Kawata, S., Ed.; Springer: Berlin, Heidelberg, 2001; pp 163–187.

- (22) Sun, S. G.; Christensen, P. A.; Wieckowski, A. *In-Situ Spectroscopic Studies of Adsorption at the Electrode and Electrocatalysis*; Elsevier: New York, 2011.
- (23) Zhu, S.; Jiang, B.; Cai, W.-B.; Shao, M. *J. Am. Chem. Soc.* **2017**, *139*, 15664–15667.
- (24) Bao, D.; Zhang, Q.; Meng, F. L.; Zhong, H. X.; Shi, M. M.; Zhang, Y.; Yan, J. M.; Jiang, Q.; Zhang, X. B. *Adv. Mater.* **2017**, *29*, 1604799.
- (25) Erikson, H.; Sarapuu, A.; Tammeveski, K.; Solla-Gullón, J.; Feliu, J. M. *ChemElectroChem* **2014**, *1*, 1338–1347.
- (26) Dunwell, M.; Yan, Y. S.; Xu, B. *Surf. Sci.* **2016**, *650*, 51–56.
- (27) Wang, X. F.; Andrews, L. *Angew. Chem., Int. Ed.* **2003**, *42*, 5201–5206.
- (28) Juarez, R.; Parker, S. F.; Concepcion, P.; Corma, A.; Garcia, H. *Chem. Sci.* **2010**, *1*, 731–738.
- (29) Enders, D.; Nagao, T.; Pucci, A.; Nakayama, T.; Aono, M. *Phys. Chem. Chem. Phys.* **2011**, *13*, 4935–4941.
- (30) Barzetti, T.; Selli, E.; Moscotti, D.; Forni, L. *J. Chem. Soc., Faraday Trans.* **1996**, *92*, 1401–1407.
- (31) Lin, S. D.; Gluhoi, A. C.; Nieuwenhuys, B. E. *Catal. Today* **2004**, *90*, 3–14.
- (32) Ramis, G.; Yi, L.; Busca, G. *Catal. Today* **1996**, *28*, 373–380.
- (33) Ramis, G.; Yi, L.; Busca, G.; Turco, M.; Kotur, E.; Willey, R. J. *J. Catal.* **1995**, *157*, 523–535.
- (34) Gulaczyk, W.; Kreglewski, M.; Valentin, A. *J. Mol. Spectrosc.* **2003**, *220*, 132–136.
- (35) Cai, W. B.; Wan, L. J.; Noda, H.; Hibino, Y.; Ataka, K.; Osawa, M. *Langmuir* **1998**, *14*, 6992–6998.
- (36) Wang, J. Y.; Peng, B.; Xie, H. N.; Cai, W. B. *Electrochim. Acta* **2009**, *54*, 1834–1841.
- (37) Ikezawa, Y.; Sawatari, T.; Kitazume, T.; Goto, H.; Toriba, K. *Electrochim. Acta* **1998**, *43*, 3297–3301.
- (38) Matsui, T.; Suzuki, S.; Katayama, Y.; Yamauchi, K.; Okanishi, T.; Muroyama, H.; Eguchi, K. *Langmuir* **2015**, *31*, 11717–11723.
- (39) Max, J. J.; Chapados, C. *J. Mol. Struct.* **2013**, *1046*, 124–135.
- (40) Coleman, M. M.; Lee, K. H.; Skrovanek, D. J.; Painter, P. C. *Macromolecules* **1986**, *19*, 2149–2157.
- (41) Asazawa, K.; Yamada, K.; Tanaka, H.; Taniguchi, M.; Oguro, K. *J. Power Sources* **2009**, *191*, 362–365.
- (42) Katayama, Y.; Okanishi, T.; Muroyama, H.; Matsui, T.; Eguchi, K. *ACS Catal.* **2016**, *6*, 2026–2034.
- (43) Mawhinney, D. B.; Glass, J. A.; Yates, J. T. *J. Phys. Chem. B* **1997**, *101*, 1202–1206.
- (44) Osawa, M.; Tsushima, M.; Mogami, H.; Samjeske, G.; Yamakata, A. *J. Phys. Chem. C* **2008**, *112*, 4248–4256.
- (45) Wang, J. X.; Springer, T. E.; Liu, P.; Shao, M. H.; Adzic, R. R. *J. Phys. Chem. C* **2007**, *111*, 12425–12433.
- (46) Kunimatsu, K.; Uchida, H.; Osawa, M.; Watanabe, M. *J. Electroanal. Chem.* **2006**, *596*, 169–169.
- (47) Yan, Y. G.; Li, Q. X.; Huo, S. J.; Ma, M.; Cai, W. B.; Osawa, M. *J. Phys. Chem. B* **2005**, *109*, 7900–7906.
- (48) Miyake, H.; Ye, S.; Osawa, M. *Electrochem. Commun.* **2002**, *4*, 973–977.
- (49) Wang, H.; Jiang, B.; Zhao, T. T.; Jiang, K.; Yang, Y.-Y.; Zhang, J.; Xie, Z.; Cai, W. B. *ACS Catal.* **2017**, *7*, 2033–2041.